Physics – Uspekhi **68** (7) 675 – 690 (2025) ©2025 Uspekhi Fizicheskikh Nauk, Russian Academy of Sciences

INSTRUMENTS AND METHODS OF INVESTIGATION PACS numbers: **07.35.+k, 42.62.–b, 47.40.–x**

Passive and active laser methods for studying kinetics of nonequilibrium processes in shock tubes

A.V. Eremin

DOI: https://doi.org/10.3367/UFNe.2025.01.039836

Contents

Abstract. A shock tube is one of the most versatile and precise instruments for studying the kinetics of high-temperature reactions in gaseous and heterogeneous media. The possibilities of detailed analyses of nonequilibrium processes occurring behind shock waves are completely determined by the use of a variety of modern diagnostic methods. Among them, various laser methods occupy a special place. As laser technologies develop, their capabilities are significantly expanded and, accordingly, new methods for their application are developed. This review presents the features of using various passive and active laser methods for studying the kinetics of nonequilibrium processes behind shock waves. Examples of the application of various laser methods are given, illustrating the wide possibilities and rich prospects for studying complex nonequilibrium processes that open up when combining a shock tube with modern laser technology.

Keywords: shock tubes, shock waves, lasers, diagnostics, passive methods, active methods, nonequilibrium processes, kinetics

1. Introduction

A shock tube is a relatively simple and at the same time reliable tool for studying nonequilibrium processes in gaseous media in a wide range of temperatures, pressures, and mixture compositions. The main advantages of a shock tube are the high homogeneity of the parameters behind the shock wave, as well as the ability to vary them over a wide range and accurately determine them by changing the intensity of the shock wave and measuring its velocity. The design and operating principle of a shock tube are quite simple (Fig. 1). It is an ordinary tube consisting of two sections separated by a diaphragm. The longer section (low-pressure chamber, LPC) is filled with the mixture under study, and the other section (high-pressure chamber, HPC) is filled with a driving gas at increased pressure, and when the diaphragm ruptures, a shock wave is formed, which, having reached the end of the tube, is reflected and forms a so-called plug of stationary shock-heated gas, where, as a rule, various nonequilibrium processes are studied.

The first attempts to create laboratory setups for studying shock waves were made more than 100 years ago [1]. However, serious interest in the shock tube as a tool for studying gas-dynamic and kinetic processes in high-temperature gas appeared only after the end of World War II. It is interesting to note that one of the world's first shock tubes was invented in the Soviet Union. In the early 1950s, postgraduate student in the Physics Department of Moscow State University T.V. Bazhenova* and undergraduate R.I. Soloukhin (Fig. 2) studied the formation of shock waves during the movement of a piston in a tube under high pressure. One day, they forgot to put the piston in the tube and were surprised to discover that the shock wave was perfectly initiated simply by rupturing the diaphragm. This is how one of the world's first modern shock tubes came into being [2, 3].

It should be noted that, at almost the same time, shock tubes began to be actively designed in many other labora-

A.V. Eremin
Joint Institute for High Temperatures, Russian Academy of Sciences, ul. Izhorskaya 13, str. 2, 125412 Moscow, Russian Federation
E-mail: eremin@jiht.ru

Received 11 November 2024, revised 9 December 2024
Uspekhi Fizicheskikh Nauk **195** (7) 721 – 737 (2025)
Translated by V.L. Derbov

* Tatyana Valerianovna Bazhenova lived a long life, passing away three weeks short of her 100th birthday. For many years, she headed the Department of Physical Gas Dynamics at the Joint Institute for High Temperatures of the Russian Academy of Sciences, which she had created. Throughout the world, she was called the "grandmother of the shock tube."

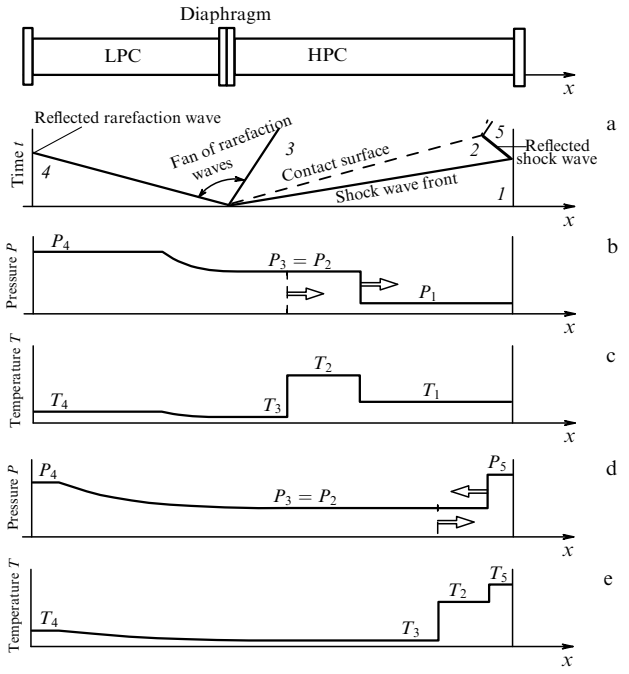

Figure 1. Structure and operation diagram of shock tube: (a) x–t diagram of shock wave propagation, contact surface, and fan of rarefaction waves at certain moment in time; (b, c) pressure profiles at certain moment after diaphragm rupture; (d, e) pressure and temperature profiles at certain moment after reflection of shock wave from end of tube.

Figure 2. Inventors of one of the world's first shock tubes: Tatyana Valerianovna Bazhenova (24.07.1923–01.07.2023) and Rem Ivanovich Soloukhin (19.11.1930–06.01.1988).

tories in different countries around the world (see reviews [4–6]). Initially, shock tubes were used to study the gas-dynamic properties of shock waves, and then experimental physicists very quickly appreciated what a remarkable tool this was for studying the kinetics of nonequilibrium processes at high temperatures [7].

Following this, several monographs appeared [8–11], describing in detail the capabilities of shock tubes for studying nonequilibrium processes in high-temperature gas, with which a new generation of researchers studying the kinetics of high-temperature reactions in shock tubes grew up. At that time, a breakthrough was made in the study of relaxation processes behind shock waves, and

Figure 3. Staly Andreevich Losev (11.07.1930–10.06.2015), the founder of Soviet school of research into nonequilibrium processes in shock tubes.

the NIST database [12] quickly began to fill up with data on the rate constants of chemical and ionization processes.

However, in the early 1970s, there was a rapid development of laser technology, and many laser methods for studying nonequilibrium processes appeared. During these years, S.A. Losev, one of the world's recognized leaders in the study of relaxation processes in shock waves (Fig. 3), regularly held schools on physicochemical kinetics. And, at one of these schools describing the capabilities of new laser methods, S.A. Losev stated that perhaps the era of shock tubes was becoming a thing of the past. Indeed, when comparing, for example, the pump-probe technique, in which two lasers operating in a frequency mode with a variable delay immediately plot a kinetic curve of the reaction being studied on the oscilloscope screen, with the shock tube technique, where at least an hour is required to obtain each point and about a month to obtain the entire kinetic curve, there was a feeling that shock tubes were no longer needed.

However, another half century has passed, and shock tubes have not sunk into the past [13], because no other experimental methods allow almost instantaneous creation of a uniformly heated volume of gas mixture with high accuracy and over wide ranges of variation in temperature, pressure, and mixture composition. A recent review [14] summarized some of the modern capabilities and lines of research in shock tubes.

So, from the point of view of research into nonequilibrium processes, the prospects turn out to be much more optimistic

if combining the capabilities of shock tube technology with those of various laser methods. This review is devoted exactly to the various possibilities that a combination of a shock tube and modern laser technology opens.

It should be noted that shock tube experiments in different laboratories are accompanied by a rich variety of different diagnostic tools, which are by no means limited to laser technology, starting with piezoelectric sensors and ionization sensors; a special place is occupied by various emission and absorption spectroscopic measurements in various spectral regions. In addition, methods of mass spectrometry, chromatography, etc. are used. All these methods are beyond the scope of this review. Moreover, various methods of laser diagnostics are successfully used to study gas-dynamic processes in shock waves, which is also beyond the scope of this review, which is devoted to the use of various laser methods to study the kinetics of nonequilibrium processes in shock tubes.

In this review, we have conditionally divided the laser methods used into passive and active ones, meaning that in passive methods only the change in the characteristics of the laser beam itself is recorded when passing through the medium under study, whereas, in active methods, the laser-induced changes in the medium under study are recorded.

2. Methods of passive laser diagnostics

2.1 Laser schlieren method

One of the first laser methods used to study the kinetics of nonequilibrium processes in shock tubes was the so-called laser schlieren method. The essence of the method is very simple and consists in deflecting a light beam by density gradients. Such methods are widely and successfully used in gas dynamics. It is obvious that, if a laser beam is passed through a shock tube cross section, it will be sharply deflected when the shock wave front passes. So, if we install a narrow diaphragm in front of the radiation detector, we will see a sharp decrease in the signal over a short time determined by the thickness (and possible curvature) of the wave front and the velocity of its propagation, as well as by the thickness of the laser beam itself. Typically, this time is about 1 μs. However, if reactions occur behind the shock wave that give rise to a change in the density of the medium, the schlieren signal will also register them, and its shape can be used to determine the kinetics of the processes taking place. The deflection angle Θ of the laser beam is related to the density gradient by a simple formula:

$$\Theta = \frac{3}{2} K_{\mathrm{L}} W \frac{\mathrm{d}\rho}{\mathrm{d}z} . \tag{1}$$

Here, K_{L} is the refractive index of the medium, and W is the width of the shock tube. The density gradient $\mathrm{d}\rho/\mathrm{d}z$ directly reflects the rate of the reaction accompanied by a change in the medium temperature.

This method was developed by John Kiefer back in the 1960s [15], and many remarkable results were obtained with its help. Figure 4a shows an example of what the laser-schlieren signals registered in one of Kiefer's first studies in 1966 during vibrational relaxation of hydrogen looked like [16]. A sharp peak of the signal near 20 μs at the moment of passage of the shock wave front is clearly visible, and the subsequent smooth descent of the signal to 25 μs precisely reflects the change in gas density during the vibrational relaxation of hydrogen. Figure 4b shows the Landau–Teller dependence of the vibrational relaxation of hydrogen obtained in this study.

Later, J. Kiefer summarized the capabilities and achievements of the laser-schlieren method in shock-tube studies of nonequilibrium processes in the monograph [17].

Note that this method, despite its integral nature, is still used in studies of the kinetics of high-temperature reactions behind shock waves.

2.2 Laser absorption spectroscopy

But, of course, a much more precise and informative method is that of laser absorption spectroscopy. This method is based on the resonant absorption of radiation of a given wavelength by specific molecules or radicals and, thus, allows one to record changes in their concentration during reactions behind shock waves. It is important to emphasize that, unlike the laser-schlieren method, such diagnostics are entirely based on the latest achievements in laser technology.

The recognized leader in the development of various methods of laser diagnostics in shock tubes is the laboratory of Ronald Hanson [18] (Fig. 5) from Stanford University,

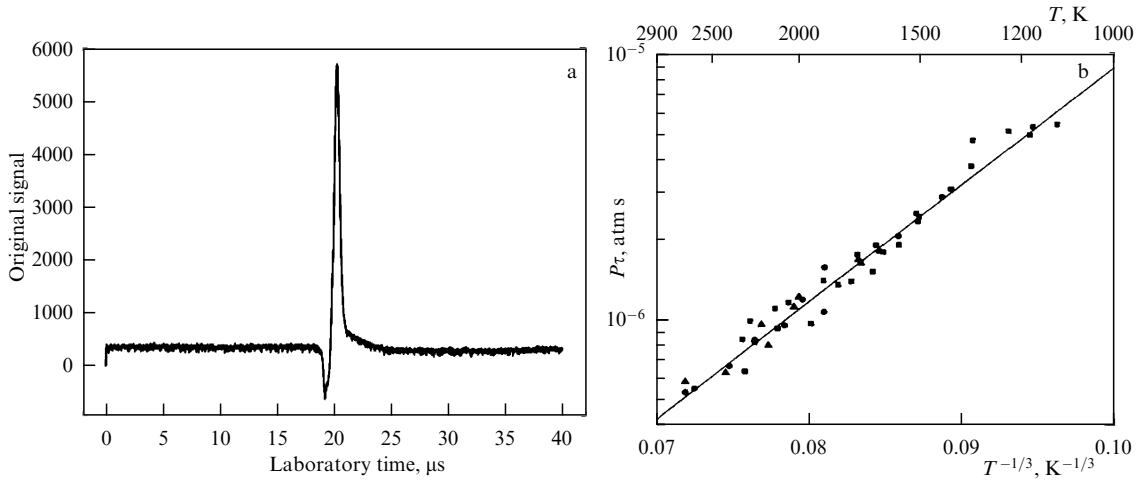

Figure 4. (a) Laser-schlieren signal behind shock wave in mixture of 50% H_2 + 50% Ar, $T = 2011$ K, $P = 0.5$ atm. (b) Landau–Teller dependence of vibrational relaxation of hydrogen [16].

Figure 5. Prof. Ronald K. Hanson (born 1939), Stanford University, a recognized leader in development of various methods of laser diagnostics in shock tubes [18].

where laser absorption spectroscopy methods have undergone the greatest development [19–21].

Figure 6 shows an example from [21] of using multichannel laser absorption diagnostics to study the kinetics of hydrocarbon pyrolysis and ignition processes behind shock waves. It is clearly seen that the authors used a large arsenal of different

Table. List of various molecules and radicals that can be diagnosed using laser absorption technology in various spectral ranges [21].

Ultraviolet		Visible		Infrared	
CH_3	216 nm	CN	388 nm	H_2O	2.5 μm
NO	225 nm	CH	431 nm	CO_2	2.7 or 4.3 μm
O_2	227 nm	NCO	440 nm	$T(t)$	2.7 + 4.3 μm
HO_2	230 nm	NO_2	472 nm	CH_4	3.4 μm
H_2O_2	230 nm	NH_2	597 nm	CH_2O	3.4 μm
OH	306 nm	HCO	614 nm	OC	4.6 μm
NH	336 nm	O_2	670 nm	NO	5.2 μm
				CH_3OH	9.6 μm
				C_2H_4	10.5 μm
				C_3H_6	10.9 μm

lasers, including gas and diode IR lasers, an He–Ne laser at various harmonics, a ring dye laser, and quantum cascade lasers. This technique made it possible to simultaneously measure the temperature of the mixture, the time profiles of the concentrations of initial hydrocarbon, and multiple intermediate radicals and products during the reaction.

The Table presents the various diagnostic components of the mixture that can be recorded using laser absorption technology in the UV, visible, and IR spectral regions.

Another impressive example is shown in Fig. 7, which demonstrates the results of simultaneous measurements of five concentrations during the oxidation of n-dodecane. It is important to note that the time in this plot is given on a logarithmic scale, making it clear how the authors managed to separately resolve the stages of pyrolysis, intermediate oxidation, and ignition.

It is important to emphasize that multichannel measurements of the time profiles of the concentrations of intermediate reaction components (intermediates) in the ignition processes of complex hydrocarbon fuels using laser absorption diagnostics make it possible to significantly improve the predictive capabilities of kinetic combustion models that include hundreds of elementary reactions.

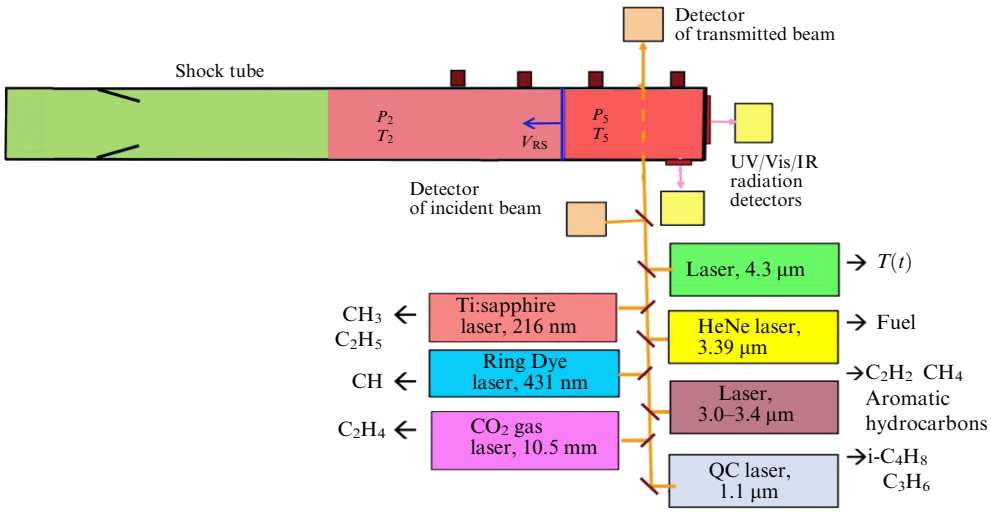

Figure 6. Application of multichannel laser absorption diagnostics to study kinetics of pyrolysis and ignition of hydrocarbon compounds behind shock waves at Stanford University [21].

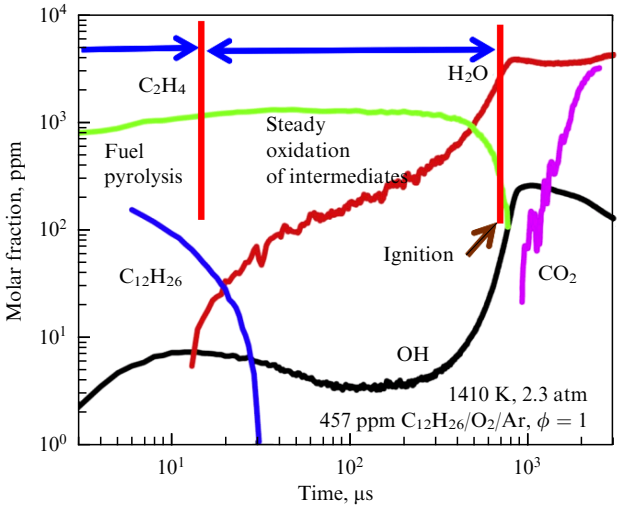

Figure 7. Example of simultaneous measurements of concentrations of 5 components of a mixture during oxidation of n-dodecane behind shock wave. Logarithmic time scale allows clear separation of stages of pyrolysis, intermediate oxidation, and ignition [21].

On the other hand, it should be noted that this technique is still very complex and quite expensive; nevertheless, it is obvious that the prospects for studying various complex nonequilibrium processes in shock tubes lie precisely in this area. Some examples of possible promising directions for the development of laser-absorption methods for studying various classes of nonequilibrium processes in shock tubes can be found in Refs [22–26].

2.3 Laser extinction

Let us now return from such fine methods of measuring individual concentrations to two more rough integral methods of laser diagnostics, the specificity of which is their applicability to the study of heterogeneous systems, i.e., systems where condensed nanoparticles are formed in the gas phase.

The first of these methods, laser extinction, is a very simple and at the same time quite sensitive tool for recording the appearance of condensed particles during chemical reactions in a shock-heated gas. The essence of the method is based on the significantly high refractive index of condensed particles compared to the gas medium. The specific feature of the laser beam passage through a gas medium with particles is that, in addition to absorption, condensed particles scatter radiation, so the total attenuation of the transmitted radiation is determined by the complex refractive index of the particles

$$m = n + \mathrm{i}k\,, \tag{2}$$

where the real n and imaginary k parts reflect the contributions of scattering and absorption to the attenuation (extinction) of the transmitted radiation. In the Rayleigh approximation, i.e., when the particle size is much smaller than the wavelength, the refractive index of the particles is completely determined by absorption and the extinction coefficient of the particles ε can be expressed as [27]

$$\varepsilon = -\frac{6\pi}{\lambda}\,\mathrm{Lm}\left\{\frac{m^2-1}{m^2+2}\right\}. \tag{3}$$

The second peculiarity of such measurements is that, usually even at a fixed point in time, the mixture contains particles of different sizes. In this regard, the measured extinction level is usually associated with the total volume of condensed particles in the mixture, expressed as the volume fraction of the condensed phase f_V. In the case of spherical particles, the volume fraction of the condensed phase can be expressed as

$$f_V = \frac{\pi}{6}\int p(d)\,d^3\,\mathrm{d}d\,, \tag{4}$$

where $p(d) = \mathrm{d}N/\mathrm{d}d$ is the particle size distribution, and N is the number density of particles of a given size d. In the case of monodimensional spherical particles, their volume fraction is

$$f_V = \frac{\pi}{6}\,Nd^3\,, \tag{5}$$

and the extinction level, defined as the attenuation of transmitted radiation, is determined in accordance with the Lambert–Beer law:

$$\frac{I}{I_0} = \exp\left(-lf_V\,\varepsilon\,(m,\lambda,d)\right), \tag{6}$$

where l is the beam path length in the absorbing medium, and λ is the wavelength of the probing radiation.

Figure 8 shows an example of a typical He–Ne laser absorption signal during benzene pyrolysis behind a shock

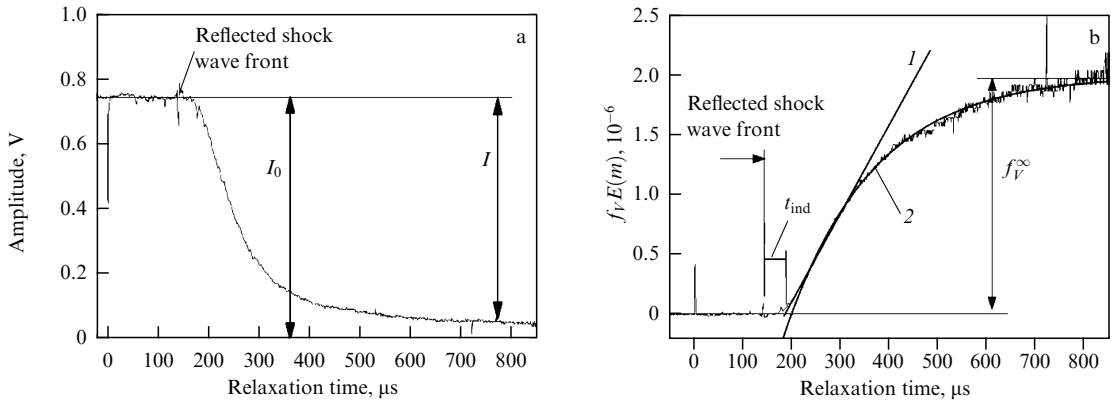

Figure 8. (a) Typical oscillogram of laser extinction during pyrolysis of benzene behind a shock wave, (b) its analysis. Mixture: 1% C_6H_6 + Ar, $T = 2000$ K, $P = 3$ bar [28].

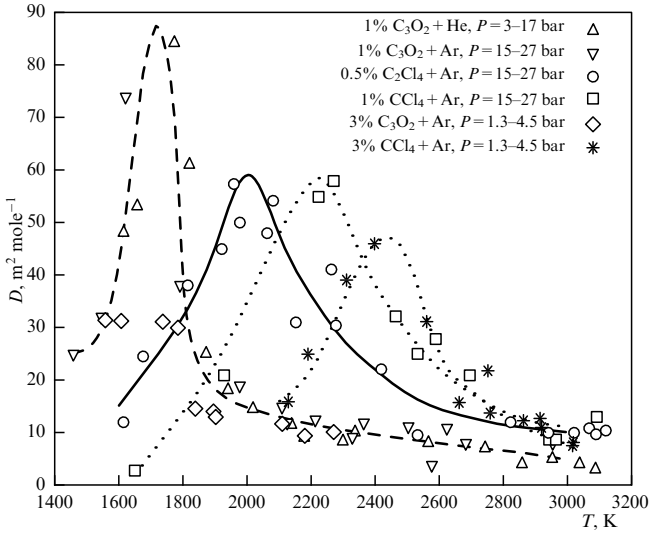

Figure 9. Temperature dependence of normalized optical density of condensed carbon particles $D = f_V \varepsilon / [C]$ ($[C]$ is total concentration of carbon in mixture) during shock-wave pyrolysis of various hydrogen-free carbon compounds [32].

wave and the characteristics of the condensed carbon nanoparticle formation process extracted from it [28].

As shown in Fig. 8, three key parameters of the condensed particle formation process can be extracted from the analysis of this signal: the induction time of the condensed phase appearance t_{ind} (the intersection of tangent *1* to the signal profile with the time axis in Fig. 8), the current and final (f_V^{∞}) value of the particle volume fraction *2*, and the effective particle growth rate constant k_{f}, determined under the assumption that the process is described by a relaxation-type equation,

$$\frac{\mathrm{d}f_V}{\mathrm{d}t} = k_{\text{f}} (f_V^{\infty} - f_V) . \qquad (7)$$

Using the laser extinction method, a huge amount of data on the processes of formation of various carbon, metal, and even complex (e.g., metal-carbon) particles was obtained (see, e.g., [29–31] and references therein).

Figures 9–11 show some examples of the most important temperature dependences of condensed particle formation obtained by measuring laser extinction in pyrolysis processes behind shock waves. Figure 9 presents the bell-shaped temperature dependences of the normalized optical density characterizing the volume fraction of particles formed during the pyrolysis of hydrogen-free carbon compounds [32]. It should be noted that the physical reasons for the formation of such bell-shaped temperature dependences of the volume fraction of condensed particles observed during shock-wave pyrolysis of any carbon compounds are still under discussion. Qualitatively, according to modern concepts, the left, low-temperature branch of this dependence reflects an increase in the degree of dissociation of the original molecules with increasing temperature, and the right, high-temperature branch is due to a decrease in the probability of formation of condensed particles with a further increase in temperature [33, 34]. The temperature shifts of the 'bells' observed in Fig. 9 reflect different thermal effects of the pyrolysis of different mixtures.

Figure 10 shows examples of the Arrhenius temperature dependence of the induction periods of particle formation, the

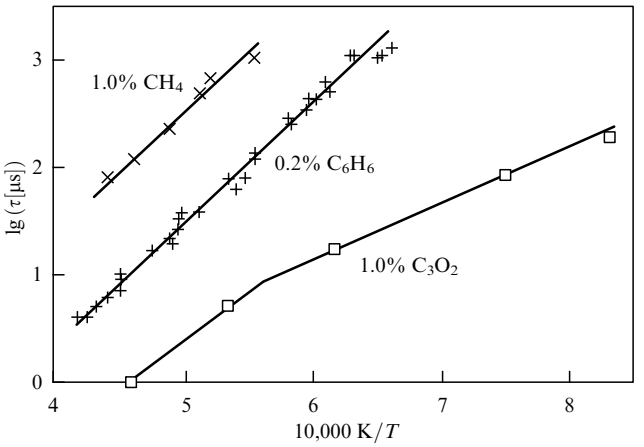

Figure 10. Arrhenius temperature dependence of induction periods of particle formation during shock-wave pyrolysis of various compounds [35].

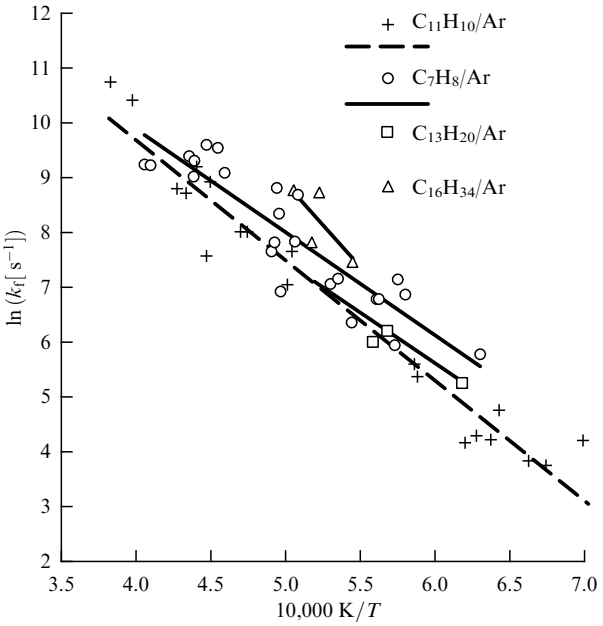

Figure 11. Arrhenius temperature dependence of effective rate constant of particle growth during shock-wave pyrolysis of various hydrocarbons [36].

slope of which reflects the effective activation energy of the bottleneck of the pyrolysis processes of various compounds. In practice, such a bottleneck is usually the primary dissociation reactions of the original molecules, which have the highest endothermicity [29, 35].

Figure 11 shows experimental data on the effective growth rate constant of condensed particles (7) during shock-wave pyrolysis of various hydrocarbon compounds, indicating a similar mechanism of particle growth regardless of the type of original hydrocarbon [36]. Note that additional confirmation of this conclusion was obtained later by laser-induced incandescence measurements, presented below among the active laser diagnostic methods.

In addition to the above characteristics of particle growth, simultaneous measurements of laser extinction at different wavelengths provide information on changes in the optical properties of particles during their formation. The oscillogram (Fig. 12) clearly shows how the absorption spectrum of

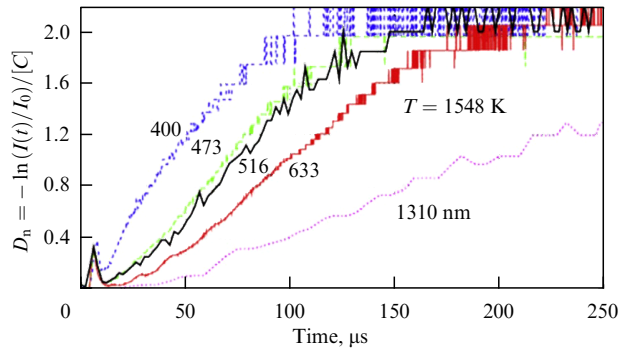

Figure 12. Example of simultaneous measurements of laser extinction at different wavelengths during pyrolysis of 1% C_3O_2 mixture in Ar behind reflected shock wave. $T = 1548$ K, $P = 28$ bar [37].

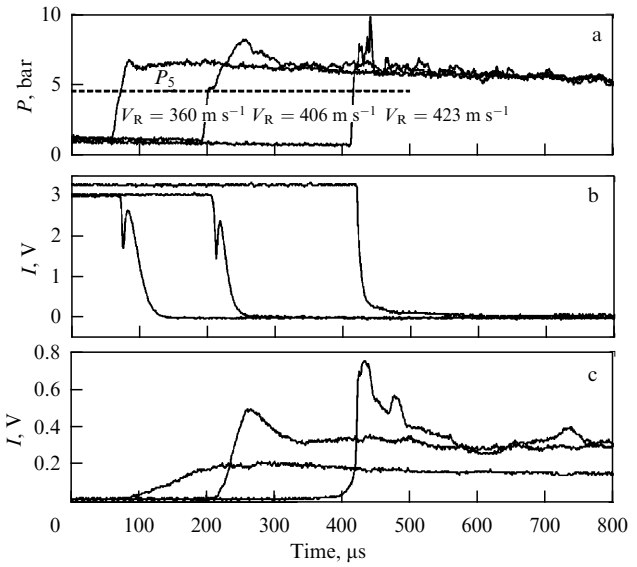

Figure 13. Oscillograms of pressure (a), laser extinction (b), and radiation (c) at $\lambda = 633$ nm behind reflected shock wave in 10% $C_3O_2 + 90\%$ Ar mixture at distances of 28 mm, 85 mm, and 195 mm from end of tube. Frozen parameters behind front of reflected shock wave: $T_5 = 1620 \pm 20$ K and $P_5 = 4.5$ atm [38].

particles expands from the UV to the IR region as they grow [37]. The reasons for the observed change in the absorption spectrum of carbon particles as they grow, as well as the temperature of their formation, were thoroughly analyzed in recent study [34].

Finally, measurements of laser extinction during condensation of carbon particles behind shock waves allowed the authors to discover a new physical phenomenon, the formation of a detonation condensation wave [38]. While studying the kinetics of shock-wave pyrolysis of exothermic carbon compounds (C_3O_2 and C_2H_2), the authors noticed that, as the shock wave propagates, the rate of extinction growth increases sharply, the wave accelerates, and pressure and radiation peaks characteristic of detonation appear in the wave front (Fig. 13). The essence of the discovered phenomenon is that the initiating shock wave propagating along the exothermic carbon compound, as a result of its rapid dissociation, forms a highly supersaturated carbon vapor, the condensation of which releases energy that forms and maintains the detonation wave. A detailed analysis of this phenomenon is given in review [39].

We add that, due to its simplicity and high sensitivity, laser extinction remains a popular and informative method for diagnosing the processes of condensed nanoparticle formation during high-temperature reactions behind shock waves [40, 41].

2.4 Laser scattering

One more method of passive laser diagnostics used to study the processes of formation or sublimation of condensed particles behind shock waves is laser scattering. Since, as already noted, this is usually Rayleigh scattering, its amplitude is very small, and it is necessary to use lasers with sufficiently high power. The intensity of the scattered radiation in the Rayleigh approximation can be written as follows [29]:

$$S_{VV} = \eta\, Q_{VV}\, I_{0,V}\, \Delta Q\, \Delta V, \tag{8}$$

where η and ΔQ are the efficiency and the aperture solid angle of the recording system, $I_{0,V}$ is the incident radiation flux, ΔV is the scattering volume, and Q_{VV} is the scattering coefficient depending on the particle size to the sixth power d^6:

$$Q_{VV} = \frac{\pi^4}{4\lambda^4}\left|\frac{m^2-1}{m^2+2}\right| N \int_0^\infty p(d)\, d^6\, \mathrm{d}d. \tag{9}$$

The strong dependence of the scattering signal on the particle size, on the one hand, allows achieving a high sensitivity of measurements to any change in the particle size, but, on the other hand, it sharply limits the minimum particle size that can be measured.

The first series of studies on measuring the sizes of carbon particles formed in the processes of pyrolysis behind shock waves using the laser scattering method was carried out by Graham and Homer [42, 43]. Later, similar measurements were reported in other papers [44–47]. The most informative ones are simultaneous measurements of scattering and extinction [45, 47]. Figure 14a shows an example of organizing such measurements in [47], where a high-power Ar laser at $\lambda = 488$ nm was used for scattering, and a conventional He–Ne laser at $\lambda = 633$ nm, for extinction. Figure 14b presents an example of the particle size time profile during heptane pyrolysis, obtained in Ref. [44] from scattering measurements. It is seen that the scattering method can be used to register particles larger than 5–10 nm.

3. Active methods of laser diagnostics

3.1 Laser-induced incandescence

All the methods described above are based on recording changes in the parameters of the laser beam as it passes through the studied medium, and they do not consider changes in the medium itself under the influence of laser radiation. Therefore, they belong to so-called methods of passive diagnostics. Let us now consider methods based on recording changes in the parameters of the studied medium under the action of a laser pulse.

Since the methods of studying gaseous media that contain condensed nanoparticles were considered above, we will start with the method of laser-induced incandescence (LII), which has become widespread in recent years for analyzing the processes of nanoparticle formation in a gaseous medium.

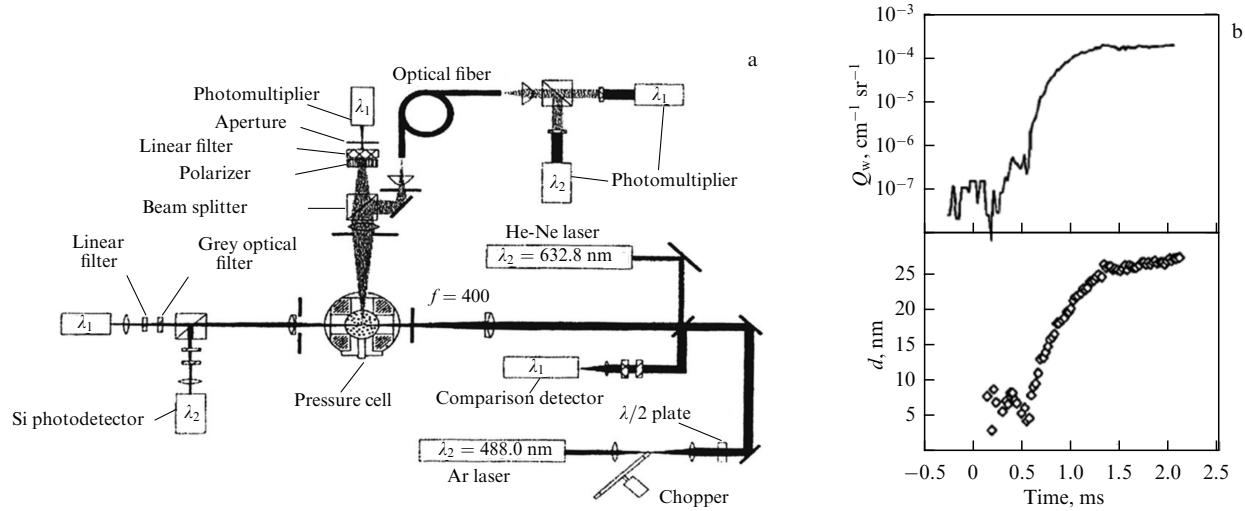

Figure 14. (a) Schematic diagram of simultaneous measurements of laser scattering and extinction behind shock waves [47]. (b) Oscillogram of scattered radiation intensity measured during pyrolysis of n-heptane in [44] and growth in size of particles extracted from it.

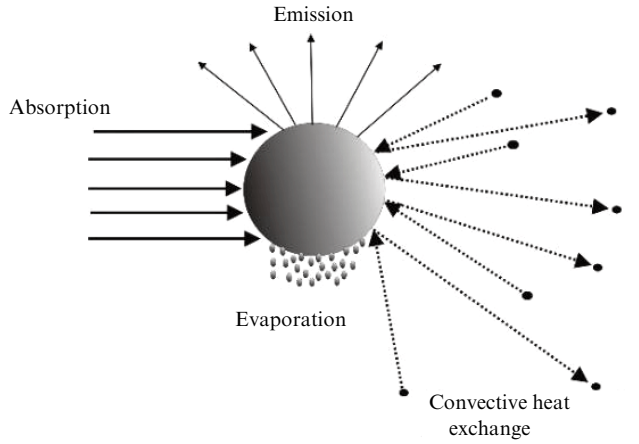

Figure 15. Schematic diagram of heat exchange of nanoparticles in processes of heating with a laser pulse and subsequent cooling.

The essence of the method consists in pulsed laser heating of nanoparticles significantly above the temperature of the surrounding gas and measuring the intensity of their thermal radiation (incandescence) that occurs as a result of the heating. The method was first proposed in 1984 by Lynn Melton [48] and was initially used to study soot formation processes in flames and later began to be used in shock tubes. At present, the LII method is successfully used for detailed studies of the formation processes and various properties of not only carbon but also metal and complex metal-carbon nanoparticles in shock waves [49–52].

Analysis of the registration data of laser-induced incandescence signals is based on solving the equation for the balance of energy and mass of particles during their heating by a laser pulse and subsequent cooling. In the general case, the intensity and time profile of incandescence depend on the thermophysical properties of nanoparticles, such as heat capacity, density, particle size, volume fraction, and refractive index of the particle material, and on the processes of heat and mass transfer between the nanoparticles and the surrounding gaseous medium. Figure 15 shows the heat exchange diagram of nanoparticles during heating by a laser pulse and subsequent cooling.

The general LII model used to estimate the particle size or volume fraction considers the current temperature of the particles T_p during their heating and cooling based on the solution of the following energy and mass conservation equations [49]:

$$\frac{d(m_p c_p T_p)}{dt} = Q_{abs} - Q_{rad} - Q_{cond} - Q_{evap}\,,$$
$$\frac{dm_p}{dt} = -J_{evap}\,, \qquad (10)$$

where m_p and c_p are the mass and heat capacity of the nanoparticle, t is the time, J_{evap} is the rate of mass loss from the particle surface during evaporation, Q_{abs} is the laser energy per unit time absorbed by the nanoparticle, and Q_{rad}, Q_{cond}, and Q_{evap} are the rates of nanoparticle energy loss because of thermal radiation, convective heat transfer, and evaporation, respectively.

In the Rayleigh approximation, the radiation energy at a wavelength λ absorbed by a nanoparticle of diameter d has the form [49]

$$Q_{abs} = \frac{\pi^2 d^3 R_0 E(m)}{\lambda_{laser}}\,, \qquad (11)$$

where $E(m)$ is the refractive index function of the particles, and R_0 is the energy density of laser radiation.

To calculate the thermal radiation flux from the surface of nanoparticles, an expression based on Planck's law is used:

$$Q_{rad} = \pi d^2 \int_0^\infty \varepsilon_{\lambda_i} \frac{2\pi h c^2}{\lambda_i^5 \left[\exp\left(hc/\lambda_i kT\right) - 1\right]}\, d\lambda_i\,. \qquad (12)$$

Convective heat exchange of nanoparticles with the surrounding gaseous medium in the free-molecular regime is presented in the form

$$Q_{cond} = \alpha\pi d^2 \frac{p_g c\,(\gamma+1)}{8(\gamma-1)} \left(\frac{T_p}{T_g} - 1\right), \qquad (13)$$

where c is the average thermal velocity of gas molecules, p_g is the total pressure of the gas mixture, γ is the adiabatic index of

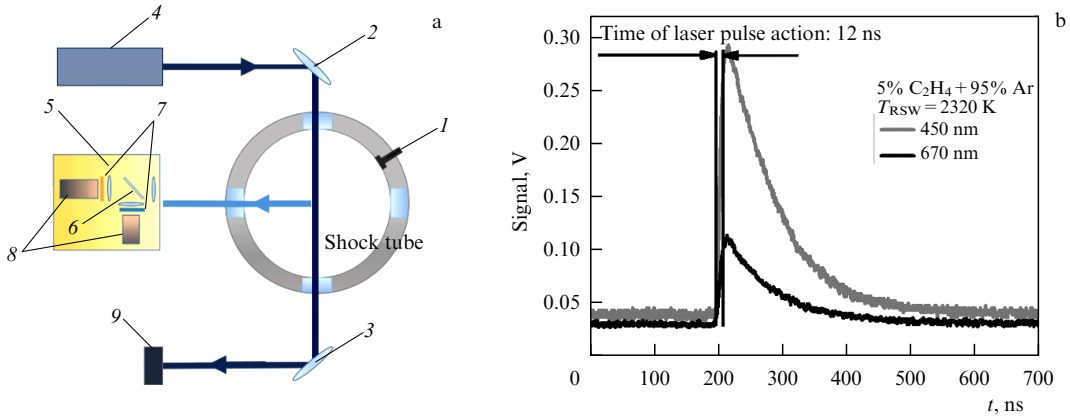

Figure 16. (a) Schematic diagram of measurements using LII method in a shock tube: *1* — pressure sensor, *2*, *3* — laser mirrors at 1064 nm, *4* — Nd:YAG laser, *5* — LII device, including: *6* — beam splitter, *7* — narrow-band optical filters, *8* — photomultiplier; *9* — pyroelectric laser energy sensor. (b) Example of experimental profile of LII signals at two wavelengths [55].

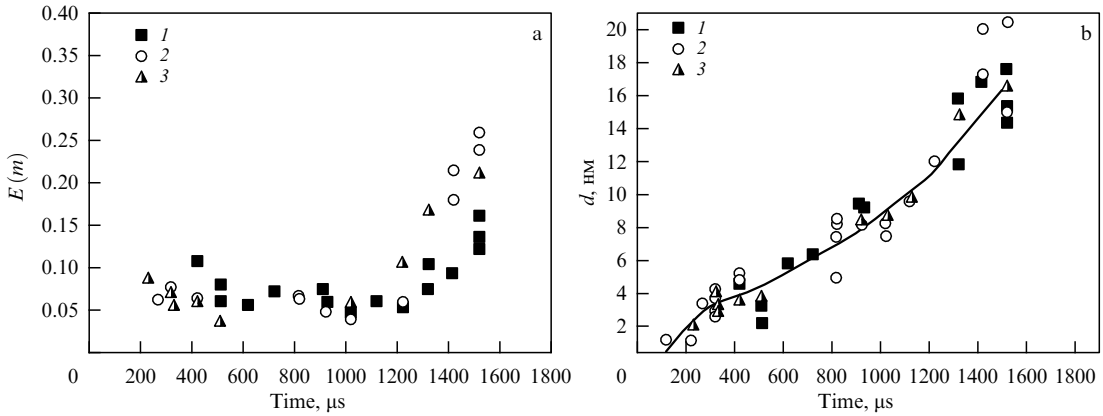

Figure 17. Growth of carbon nanoparticles during acetylene pyrolysis behind shock waves at different temperatures. (a) Function of particle refractive index, (b) average particle size. Symbols: *1*, *2*, *3* — measurements at temperatures of 1850, 1950, and 2050 K; line — approximation of experimental data [53].

the gaseous medium, α is the accommodation coefficient of the thermal energy of the surrounding gas molecules on the surface of the nanoparticles, T_p is the current temperature of the nanoparticle, and T_g is the temperature of the surrounding gas. The main uncertainty in calculating convective heat exchange in the free-molecular regime is associated with the magnitude of the accommodation coefficient. According to literature data [50], the values of this coefficient for carbon nanoparticles vary in the range from 0.23 to 0.5, depending on conditions.

If nanoparticles are heated to temperatures exceeding the evaporation temperature, then atoms or larger clusters can leave the surface of the nanoparticle. The loss of thermal energy because of evaporation depends on the molar mass of the evaporated particles W_s (atoms, clusters), the enthalpy of vaporization ΔH_V, and the rate of mass loss $\mathrm{d}m_p/\mathrm{d}t$:

$$Q_{\text{evap}} = -\frac{\Delta H_V}{W_s}\frac{\mathrm{d}m_p}{\mathrm{d}t}. \qquad (14)$$

In most practical cases, radiation cooling of nanoparticles can be disregarded, and if the particles are heated below the sublimation temperature, the main mechanism of their cooling is collisions with molecules of the surrounding gas, described by equation (13).

Recording time-resolved incandescence signals at two or more wavelengths makes it possible to determine the evolution of the particle temperature. In some cases, these measurements make it possible to determine the refractive index function of the nanoparticle material [49, 53]. In addition, with an increase in the laser radiation flux density, the peak temperature of laser-heated particles approaches their evaporation/sublimation temperature, which allows determining its real value [49, 54].

In conventional LII techniques, the volume fraction of particles or the particle size distribution are determined, on the one hand, by analyzing LII signals with the expected properties of the nanoparticles taken into account. On the other hand, if the particle size distribution and other properties are known, the analysis of the LII signals can provide various particle properties (for example, the thermal energy accommodation coefficient [49]).

Figure 16 schematically illustrates the LII measurements in a shock tube and shows a typical view of incandescence signals [55].

Figures 17 and 18 present examples of results obtained using the LII method in shock tubes. Figure 17 shows how the optical properties and particle size change during acetylene pyrolysis at different temperatures [53]. It is characteristic that the refractive index of the particles increases sharply as

their sizes increase beyond 10 nm (Fig. 17a). In Ref. [56], the process of changing the optical properties of carbon particles as they grow was studied in detail for particles formed during the pyrolysis and combustion of various hydrocarbons. It was shown that the reason for such a change in the particle properties is a significant transformation of the internal structure of soot particles in this size range from so-called 'young' to 'mature' ones, after which their structure and, accordingly, properties no longer change, and soot growth occurs mainly due to the aggregation of primary particles. In this case, a significant change in the optical properties of soot particles depending on their size correlates with a decrease in the average distance between adjacent parallel graphene planes that make up the structure of soot particles, from 0.5 nm to 0.35 nm, close to the interplanar distance in graphite (0.335 nm), with an increase in the average sizes of soot particles from 10 to 25 nm.

Another characteristic feature of the particle growth is that the rate of this process remains virtually unchanged at different temperatures (Fig. 17b). This fact indirectly indicates that, in the considered time range, particle growth occurs through barrier-free surface growth reactions. Generally, according to modern concepts, the formation of condensed particles during pyrolysis of carbon compounds can be conditionally divided into three stages. The first, the endothermic stage of dissociation of the initial molecules, the rate of which strongly depends on the temperature, under the conditions of shock-tube experiments usually lasts no more than several ten microseconds. This is followed by the stage of surface growth of particles, which lasts from hundreds of microseconds to several milliseconds, depending on the concentration of the reacting molecules, and is practically independent of temperature. The kinetic mechanism of such a process, proposed back in 1991 [57] and, despite a number of controversial issues, still considered the main mechanism of surface growth of carbon particles during hydrocarbon pyrolysis, is called HACA (Hydrogen Abstraction Carbon Addition). And the last stage of particle growth occurs through the coagulation of small particles into larger ones. This process occurs on millisecond time scales and is usually inaccessible for observation in shock tube experiments.

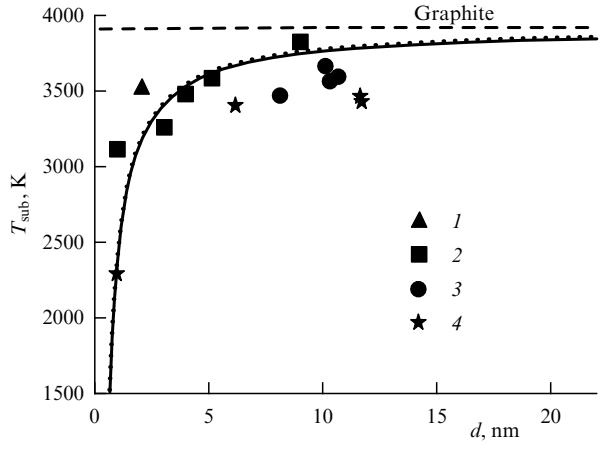

Figure 18. Change in sublimation temperature of carbon nanoparticles formed during pyrolysis of mixture of 1% C_6H_6 + 99% Ar behind shock waves, depending on particle size. Temperature behind shock wave: *1* — 2350 K, *2* — 2220 K, *3* — 2100 K, *4* — 1950 K. Curve — approximation of experimental data. Dashed straight line shows graphite sublimation temperature [54].

Figure 18 shows data on the increase in the sublimation temperature of carbon particles with an increase in their size [54]. It is evident that, also regardless of the temperature of particle formation behind the shock wave, this temperature approaches the sublimation temperature of graphite for particle sizes greater than 15 nm. It is characteristic that such a change in the thermodynamic properties of particles with an increase in their size agrees well with the change in optical properties shown in Fig. 17a and also reflects a change in the internal structure of the particles and its approach to the parameters of graphite [56].

It is worth noting that the LII method continues to develop and has become so widespread in various laboratories around the world that, since 2005, international conferences have been held every two years on the latest advances in this diagnostic method [58].

3.2 Laser-induced fluorescence

Another method of active laser diagnostics is the laser-induced fluorescence (LIF) method, which involves the transition of electrons of gas molecules of a certain type to excited states when exposed to a laser pulse and the recording of the resulting fluorescence in the spectral range characteristic of a given type of molecule. By analyzing the obtained LIF spectra (spectral region, shape, amplitude, and time profile), it is possible to identify individual molecules, their temperature, and their concentration.

Good candidates for the diagnostics of kinetic processes behind shock waves by the LIF method are heavy organic molecules with high absorption coefficients and quantum yields. The absorption of ultraviolet and visible radiation in organic molecules is determined by valence electrons with low excitation energy. The absorption spectrum of such molecules is usually broad and continuous. As a rule, the UV region of the spectrum is used to excite fluorescence.

Figure 19 shows a diagram of simultaneous LIF and laser extinction measurements on a shock tube from Ref. [59].

To excite fluorescence, the fourth harmonic of an Nd–YAG laser at $\lambda = 266$ nm was used, launched with different delays after the passage of the shock wave, which made it possible to study the change in the nature of fluorescence during the reactions. The fluorescence spectrum was recorded using a spectroscope and a CCD camera. In Ref. [59], this technique was used to study the growth of polyaromatic hydrocarbon (PAH) molecules during the pyrolysis of various hydrocarbon fuels behind shock waves. The potential of such a study was based on the significant dependence of the fluorescence spectra of PAHs on their size. Figure 20 shows all the data available in the literature on the fluorescence spectra of various PAHs, collected in Ref. [59]. It is clearly seen that the simplest aromatic hydrocarbon, benzene, has a spectrum in the 250–300 nm region, and, as the number of aromatic rings increases, the spectrum shifts to the long-wave range, and for heavy PAHs, the fluorescence spectrum is near 500 nm.

Figure 21a shows the LIF spectrum of benzene at room temperature, and Fig. 21b shows an example of the change in the fluorescence spectrum during benzene pyrolysis at different reaction times. It is clearly seen how the fluorescence spectrum shifts to the long-wave region over time, which reflects an increase in the PAH size. It should be noted that, since the LIF spectra overlap greatly for different PAHs, and on the other hand, in a real reacting mixture at any given time there is a variety of different PAHs simultaneously, the measurements in [59] naturally presented only a qualita-

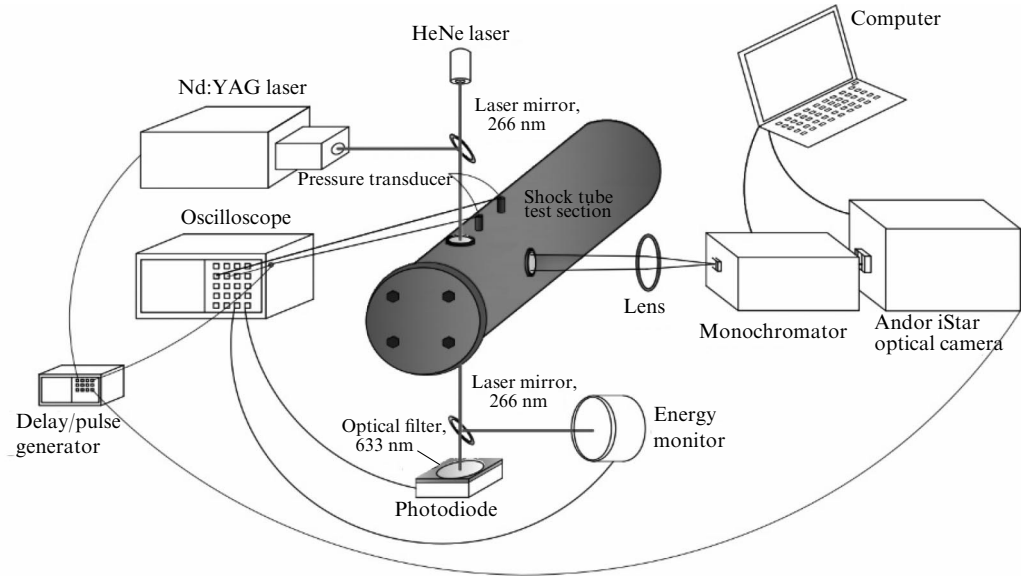

Figure 19. Schematic diagram of simultaneous measurements of LIF and laser extinction in shock tube [55].

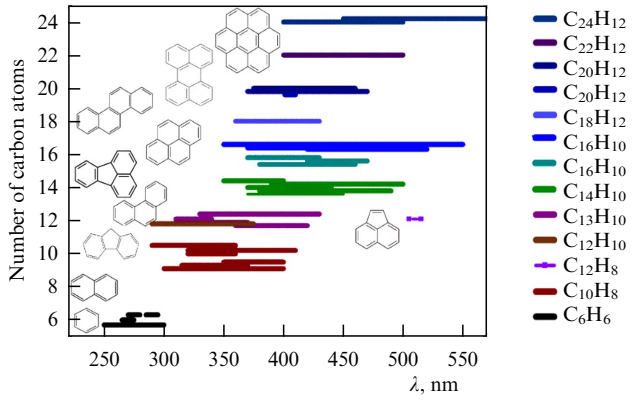

Figure 20. Spectral range of LIF of PAH, depending on number of carbon atoms [55].

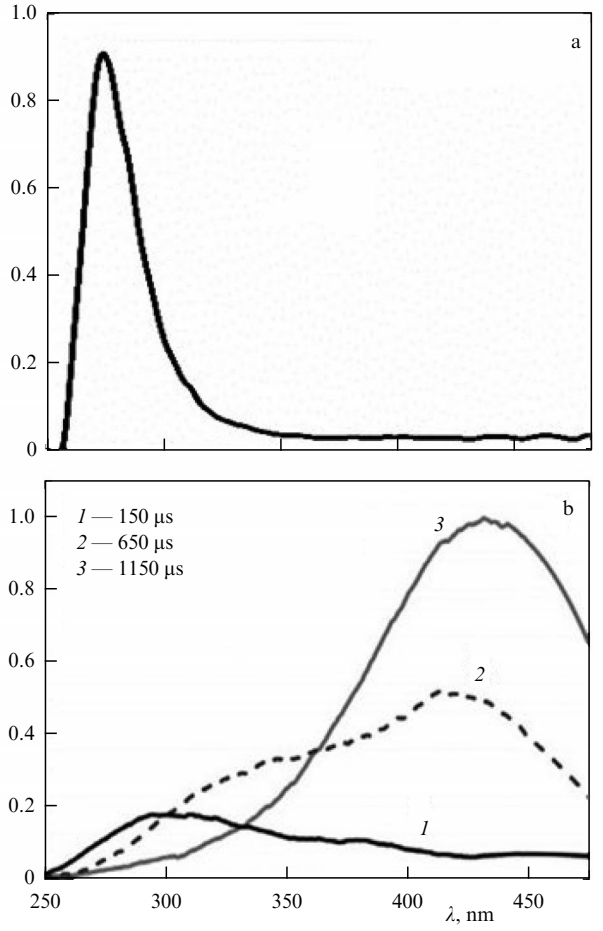

Figure 21. Fluorescence spectrum of benzene at room temperature (a) and behind a shock wave at different reaction times (b). Mixture: 1% C_6H_6 + 99% Ar; (a) $T = 295$ K, (b) $T = 1500 \pm 15$ K [55].

tive character of the PAH growth under certain conditions. Nevertheless, such studies were one of the first examples in the world of applying the LIF method under conditions of hydrocarbon pyrolysis in a shock tube and provided new interesting data on the change in the character of PAH growth upon the addition of various types of biofuels. Based on the obtained LIF spectra and laser extinction measurements, it was established in [59] that additives of a promising biofuel, dimethyl ether, accelerate the formation of small aromatic compounds consisting of 1–2 rings and slow down the formation of larger PAHs and condensed soot particles.

Further development of the LIF method for studying the kinetics of the formation of heavy hydrocarbon molecules in pyrolysis processes behind shock waves can be associated with the use of picosecond lasers and the measurement of time profiles of fluorescence intensity, usually amounting to several ten nanoseconds, which can provide more reliable information on the change in the concentration of various types of molecules during the reaction.

Another, completely different, application of the LIF effect in shock tubes was realized in some laboratories, first of all, again in the laboratory of R. Hanson, to study the development of various nonequilibrium processes along the flow field behind the shock wave front. In this case, the laser beam was shaped to form a thin light sheet in the horizontal plane along the flow in the shock tube, and, using a CCD camera, the distribution of fluorescence over the entire flow field inside the tube was recorded rather than its spectrum [60] (Fig. 22). This method was called planar LIF (PLIF). In this

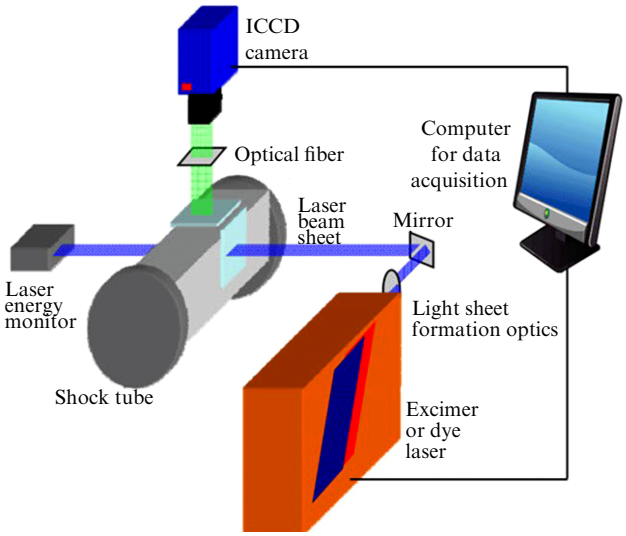

Figure 22. Schematic diagram of organization of measurements of planar laser-induced fluorescence behind shock wave front in shock tube [60].

case, various intensely emitting molecules or radicals (toluene, NO, OH, etc.) were selected to excite fluorescence and the change in LIF intensity over the flow field was analyzed.

Using the above method, the vibrational relaxation times of NO were measured [61]. For this purpose, the flow field of a 1% NO + Ar mixture in a shock tube was irradiated by a pulse from an excimer Ar–F laser operating in the single-mode regime at a wavelength of 193.34 nm, corresponding to absorption from the first vibrational level of the ground electronic state of NO molecules ($X^2\Pi$), and a CCD camera was used to record the fluorescence intensity distribution of electronically excited NO molecules ($D^2\Sigma$) in the range of 187–268 nm along the flow field behind the shock wave. The analysis of the obtained images was in good agreement with the known data on the vibrational relaxation rates of nitrogen oxide (Fig. 23).

In Ref. [62], the PLIF method was used to study the development of ignition in a combustible mixture behind the shock wave front. In this case, a combination of an excimer Xe–Cl laser and a dye laser was used to produce a pulse of radiation at a wavelength of 283 nm that excited the fluorescence of OH radicals. Figure 24 shows how the fields

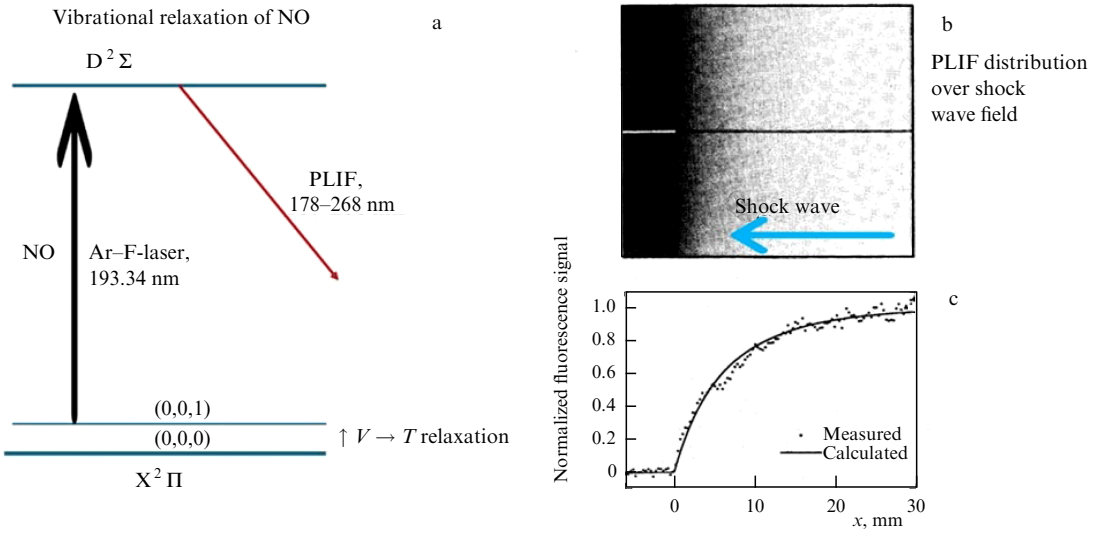

Figure 23. Application of PLIF method to record vibrational relaxation of nitrogen oxide behind shock wave front [61]. (a) Schematic diagram of NO levels excited by laser pulse and subsequent fluorescence, (b) fluorescence distribution over flow field in shock tube, and (c) extracted NO vibrational relaxation profile in comparison with calculated data.

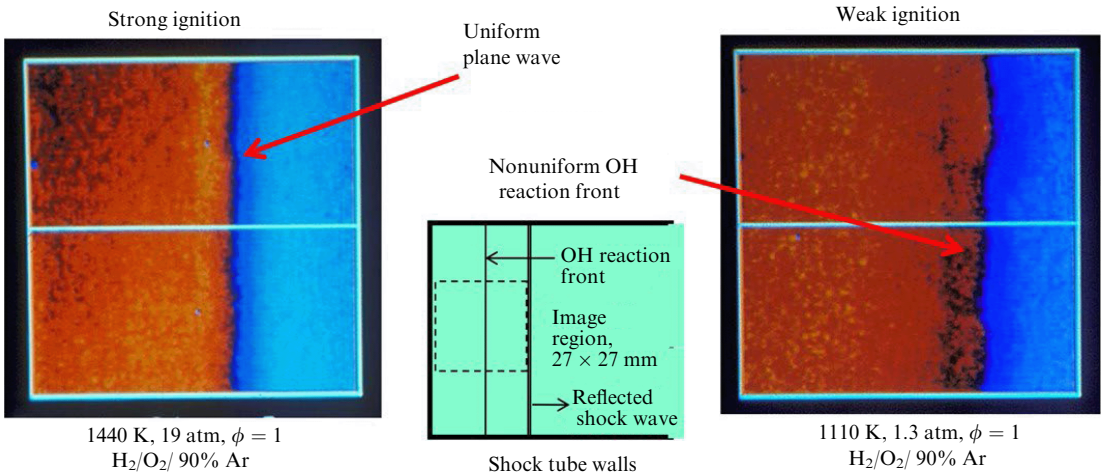

Figure 24. Application of ON-PLIF method to record development of ignition in H_2/O_2 mixture behind shock wave front [62].

of OH fluorescence at 308 nm looked for 'strong' and 'weak' ignition of an H_2/O_2 mixture behind a shock wave.

It should be noted, however, that this technique has found its greatest application in the study of complex, nonuniform flows, so its use in a shock tube is limited.

4. Combined shock-wave and laser initiation of nonequilibrium processes

4.1 Laser photolysis in shock-heated gas

The last group of active laser methods includes those where the laser action not only changes the state of individual groups of molecules or particles but initiates fundamentally new nonequilibrium processes in the shock-heated mixture. In this way, it is possible to study the kinetics of processes that arise exclusively under the combined action of a shock wave and a laser pulse.

The first example of such a complex reactor is the use of laser photolysis processes in shock-heated gas. As is known, one of the most significant limitations of the operation of a shock tube is the short time of existence of an undisturbed plug behind the reflected shock wave. Typically, this time is about 1 ms. Using 'tailoring' modes, i.e., conditions when the reflected wave, colliding with the contact surface, does not form disturbances that go back to the end of the tube, it is possible to increase this time to several ms, before the arrival of the rarefaction wave, reflected from the opposite end of the tube. Various tricks also exist to increase this time, e.g., lengthening the low-pressure chamber and even special inserts in the chamber that compensate for the pressure drop in the rarefaction wave [19, 63]. Thanks to this, as indicated in Ref. [63], it is possible to increase the working time of the shock tube to several ten milliseconds. However, one way or another, due to various dissipative processes, the constancy of the parameters in the plug noticeably worsens at millisecond times. On the other hand, most practically important nonequilibrium processes, especially combustion processes, occur at characteristic reaction times that are fractions of a second, which cannot be investigated in a conventional shock tube.

The use of pulsed laser photolysis in a plug of a shock-heated mixture can partly overcome this problem. When exposed to a laser pulse, practically regardless of the temperature and pressure in the mixture, a concentration of active atoms or radicals can be created in the volume irradiated by the laser which react with the molecules of the mixture. This method was first implemented in the late 1980s and 1990s in the USA in the laboratory of Ronald Hanson [64, 65], in Japan in the group of Hiroaki Matsui [66, 67], and in Germany in the laboratory of Paul Roth [68, 69]. At present, in Russia, at the Joint Institute for High Temperatures of the Russian Academy of Sciences, one of the current versions of such an experimental complex has been implemented for the first time. It consists of a high-vacuum kinetic shock tube and an excimer Ar–F laser at a wavelength of 193 nm, the pulse of which produces photolysis of oxygen in a plug of shock-heated gas with the formation of two O atoms [70, 71] (Fig. 25). For reliable and accurate determination of the absolute concentration of oxygen atoms under these conditions, the precision method of atomic resonance absorption spectroscopy (ARAS), called the 'gold standard' in the kinetics of high-temperature reactions, is used. Details of the measurements of the time profiles of absolute concentrations of atomic oxygen using the ARAS method behind shock waves are thoroughly described in recent article [72].

Figure 26a shows an example of a resonance absorption signal of oxygen atoms at a wavelength of 130.5 nm in a mixture of 500 ppm O_2+ argon at a temperature behind the reflected shock wave of $T_5 = 1210$ K and a pressure of $p = 3.3$ atm, as well as a signal from a pressure sensor in the same cross section for characteristic experimental parameters. Small changes in the absorption signal after the arrival of the incident and reflected shock waves are caused by the absorption of molecular oxygen at a given wavelength, and a significant increase in absorption is due to the appearance of atomic oxygen at the time of the Ar–F laser pulse. Due to the high dilution of the mixture with argon and the low concentration of O atoms, recombination processes are insignificant, and the concentration of O atoms formed by photolysis remains unchanged during the entire observation time. Figure 26b shows an oscillogram obtained at approximately the same temperature and pressure, where 10 ppm methane is added to a mixture of 1000 ppm O_2+ argon. A drop in the concentration of O atoms makes it possible to

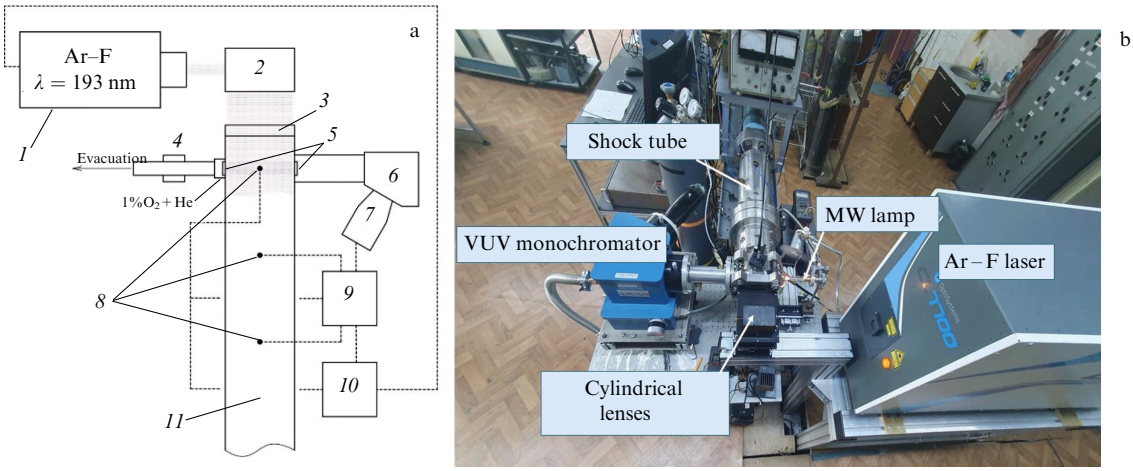

Figure 25. Schematic diagram (a) and exterior view (b) of experimental shock tube/laser photolysis complex with atomic resonance absorption system for measuring concentration of oxygen atoms. *1* — excimer laser, *2* — optical system for forming horizontal laser beam, *3* — quartz window at end of shock tube, *4* — microwave lamp with antenna from microwave generator for exciting radiation of O atoms at wavelength of 130.5 nm, *5* — MgF_2 windows, *6* — Acton-502 vacuum monochromator, *7* — FEU-181 photomultiplier tube, *8* — RSV pressure sensors, *9*, *10* — oscilloscopes, *11* — shock tube [70].

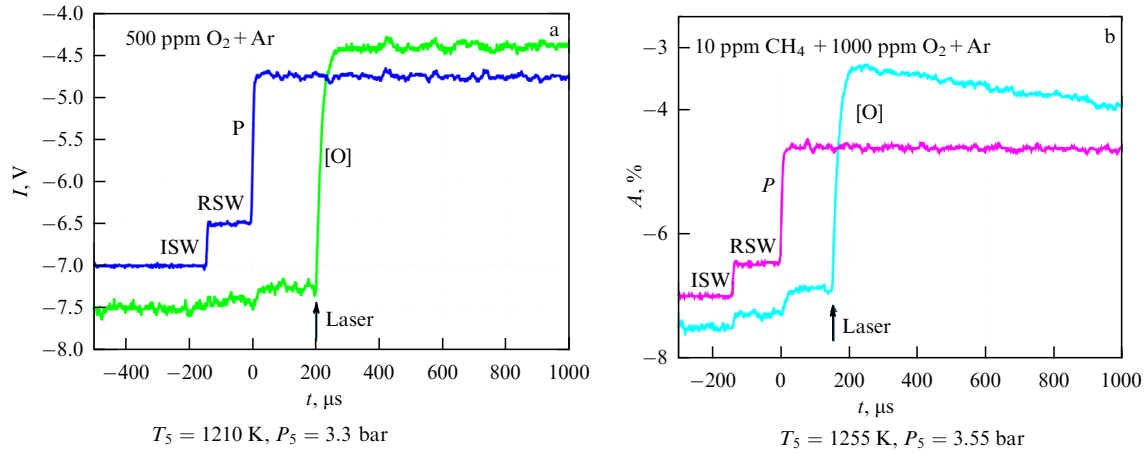

Figure 26. Examples of characteristic oscillograms of O atom concentration during laser photolysis of oxygen behind shock waves. *P* — pressure profile, ISW and RSW — fronts of incident and reflected shock waves [70].

directly determine the rate constant of the O + CH_4 reaction, and arbitrary variation of the parameters behind the shock wave makes it possible to determine the temperature dependence of the rate constant of this reaction.

The prospects for using such initiation of nonequilibrium processes under the combined action of shock-wave heating and pulsed laser photolysis are quite obvious — the use of lasers at different wavelengths can make it possible to generate a variety of active atoms or radicals, and varying the composition of the mixture and the parameters behind the shock wave makes it possible to study the kinetics of their interactions with various molecules over a wide range of temperatures and pressures.

4.2 Laser-induced spark ignition behind shock waves

Another interesting combination of a shock tube with a laser is the laser-induced spark ignition behind shock waves, proposed in Refs [73–75]. The idea of the method is to focus a laser beam pulse on the center of the tube in order to achieve point spark ignition of the combustible mixture in the plug behind the reflected shock wave. In this case, the laser energy was minimized so that ignition occurred strictly only at the beam focusing point. Then, the flame propagation process was recorded by a CCD camera through the transparent end of the shock tube. And, as in all previous methods, the main advantage of such a combination of a shock tube and a laser pulse was the ability to study the flame propagation process in a wide range of temperatures and pressures by changing the parameters behind the reflected shock wave. Figure 27a shows a diagram of the organization of such experiments [73] and an example of the obtained images of flame propagation at different moments in time, and Fig. 27b shows the dependence of the flame velocity in a methane-air mixture on temperature, obtained in Ref. [73].

Using this technique, the temperature dependences of the flame velocity were measured in a propane-oxygen mixture [74] and in an ammonia–air mixture [75].

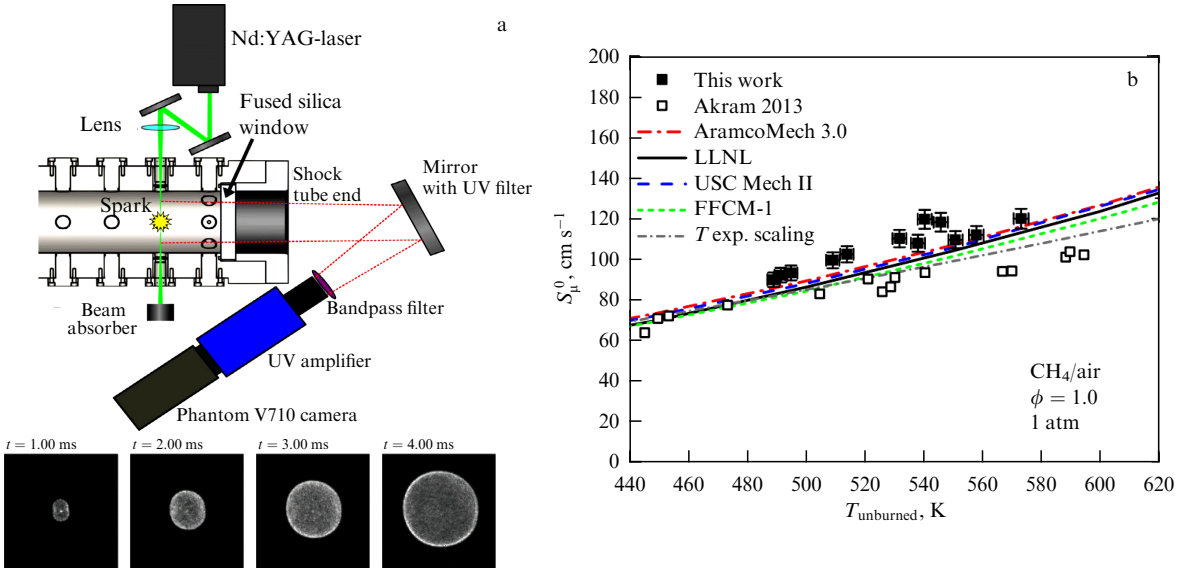

Figure 27. (a) Schematic of organization of experiments on laser-spark ignition of a combustible mixture behind a shock wave and examples of images of flame propagation at different moments in time [73]. (b) Temperature dependence of flame velocity in methane-air mixture measured using these data in comparison with results of other studies.

Obviously, such a technique has great promise from the point of view of studying the patterns of change in the flame propagation velocity in various combustible mixtures in a wide range of temperatures and pressures, which are difficult to implement in other experimental settings.

5. Conclusion

The present review shows how extensive the possibilities provided by the combination of a shock tube and modern laser technology are for studying nonequilibrium processes in various gas mixtures. At the same time, due to the continuing development of laser technology, such possibilities are increasing every year.

From the point of view of prospects in this area, the most interesting one is the progress on the development of quantum-cascade lasers, which can provide both an expansion of their spectral ranges and a reduction in price, allowing the implementation of multichannel setups for recording individual components during complex reactions.

Another interesting prospect may be the use of picosecond lasers to record time-resolved LIF signals during nonequilibrium processes behind shock waves.

In addition, we can expect new findings in joint shock-wave and laser initiation of nonequilibrium processes, which, in principle, allows the implementation of conditions that are inaccessible in any other reactors.

Acknowledgments. The study was carried out with financial support from the Russian Science Foundation (project no. 23-19-00407).

References

1. Vieille P *C.R. Acad. Sci. Paris* **129** 1228 (1899)
2. Bazhenova T V, Soloukhin R I, in *Proc. of the Seventh Intern. Symp. on Combustion* (London: Butterworths, 1959) p. 866
3. Soloukhin R I *Sov. Phys. Usp.* **2** 547 (1959); *Usp. Fiz. Nauk* **68** 513 (1959)
4. Glass I I, Gordon H J 'Shock tubes,' in *Handbook of Supersonic Aerodynamics* (Silver Spring, MD, 1959) Sect. 18
5. Rakhmatullin Kh A, Semenov S S (Eds) *Udarnye Truby* (Shock Tubes) (Moscow: IL, 1962) Collection of translated articles
6. Ferri A (Ed.) *Fundamental Data Obtained from Shock-Tube Experiments* (New York: Pergamon Press, 1961); Translated into Russian: *Osnovnye Rezul'taty Eksperimentov na Udarnykh Trubakh* (Moscow: Gosatomizdat, 1963)
7. Losev S A, Osipov A I *Sov. Phys. Usp.* **4** 525 (1962); *Usp. Fiz. Nauk* **74** 393 (1961)
8. Gaydon A G, Hurle I R *The Shock Tube in High-Temperature Chemical Physics* (New York: Reinhold Publ. Corp., 1963); Translated into Russian: *Udarnaya Truba v Khimicheskoi Fizike Vysokikh Temperatur* (Moscow: Mir, 1966)
9. Stupochenko Ye V, Losev S A, Osipov A I *Relaxation in Shock Waves* (New York: Springer-Verlag, 1967); Translated from Russian: *Relaksatsionnye Protsessy v Udarnykh Volnakh* (Moscow: Nauka, 1965)
10. Zel'dovich Ya B, Raizer Yu P *Physics of Shock Waves and High-Temperature Hydrodynamic Phenomena* (Mineola, NY: Dover Publ., 2002); Translated from Russian: *Fizika Udarnykh Voln i Vysokotemperaturnykh Gidrodinamicheskikh Yavlenii* (Moscow: Nauka, 1966)
11. Bazhenova T V et al. *Shock Waves in Real Gases* (Washington: National Aeronautics and Space Administration, 1969); Translated from Russian: *Udarnye Volny v Real'nykh Gazakh* (Moscow: Nauka, 1968)
12. National Standard Reference Data Series. National Institute of Standards and Technology, https://www.nist.gov/srd/national-standard-reference-data-series
13. Fomin N A *J. Eng. Phys. Thermophys.* **83** 1244 (2010); *Inzh.-Fiz. Zh.* **83** 1058 (2010)
14. Sakthi Balan G, Aravind Raj S *Int. J. Impact Eng.* **172** 104406 (2023)
15. Kiefer J H, Lutz R W *Phys. Fluids* **8** 1393 (1965)
16. Kiefer J H, Lutz R W *J. Chem. Phys.* **44** 668 (1966)
17. Kiefer J H, in *Shock Waves in Chemistry* (Ed. A Lifshitz) (New York: M. Dekker, 1981) p. 219
18. Davidson D F et al. *Combustion Flame* **224** 2 (2021) https://doi.org/10.1016/j.combustflame.2020.08.039
19. Hanson R K, Davidson D F *Prog. Energy Combust. Sci.* **44** 103 (2014)
20. Hanson R K *Proc. Combust. Inst.* **33** (1) 1 (2011)
21. Hanson R K, Davidson D F, in *Proc. of the 25th Intern. Colloquium on the Dynamics of Explosions and Reactive Systems, ICDERS, August 2–7, 2015, Leeds, UK*, Paper 260
22. Wang S et al. *Proc. Combust. Inst.* **39** 755 (2023)
23. Krish A, Streicher J W, Hanson R K *J. Quant. Spectrosc. Radiat. Transfer* **280** 108073 (2022)
24. Krish A, Streicher J W, Hanson R K, in *2021 Intern. Symp. on Molecular Spectroscopy* (*Virtual*) *June 21–25, 2021*, Talk FF11, https://doi.org/10.15278/isms.2021.FF11
25. Pinkowski N H et al. *Meas. Sci. Technol.* **32** 035501 (2021)
26. Chao X et al. *Proc. Combust. Inst.* **37** 1345 (2019)
27. Bohren C F, Huffman D R *Absorption and Scattering of Light by Small Particles* (New York: Wiley, 1983)
28. Eremin A, Gurentsov E, Mikheyeva E *Combust. Flame* **162** 207 (2015)
29. Eremin A V *Prog. Energy Combust. Sci.* **38** 1 (2012)
30. Gurentsov E V et al. *Kinetics Catalysis* **46** 309 (2005); *Kinetika Kataliz* **46** 333 (2005)
31. Nativel D et al. *Combust. Flame* **243** 111985 (2022)
32. Emelianov A et al. *Proc. Combust. Inst.* **30** 1433 (2005)
33. Emelianov A et al. *Proc. Combust. Inst.* **35** 1753 (2015)
34. Eremin A V et al. *High Temp.* **62** 496 (2024); *Teplofiz. Vys. Temp.* **62** 563 (2024)
35. Dörge K J, Tanke D, Wagner H Gg *Z. Phys. Chem.* **212** 219 (1999)
36. Douce F et al. *Proc. Combust. Inst.* **28** 2523 (2000)
37. Emelianov A et al. *Proc. Combust. Inst.* **29** 2351 (2002)
38. Emel'yanov A V et al. *JETP Lett.* **87** 470 (2008); *Pis'ma Zh. Eksp. Teor. Fiz.* **87** 556 (2008)
39. Eremin A V, Fortov V E *Phys. Usp.* **64** 1073 (2021); *Usp. Fiz. Nauk* **191** 1131 (2021)
40. Nativel D et al. *Proc. Combust. Inst.* **39** 1099 (2023)
41. Drakon A V et al. *Kinetika Kataliz* **65** 609 (2024)
42. Graham S C, Homer J B, in *Recent Developments in Shock Tube Research, Proc.* (Eds D Bershader, W Griffith) (Stanford, CA: Stanford Univ. Press, 1973) p. 712
43. Graham S C, Homer J B, Rosenfeld J L *Proc. R. Soc. London* **344** 259 (1975)
44. Kellerer H et al. *Combust. Sci. Technol.* **113** 67 (1996)
45. di Stasio S, Massoli P, Lazzaro M *J. Aerosol Sci.* **27** 6897 (1996)
46. Kellerer H, Wittig S, in *Proc. of the 21th Intern. Symp. Shock Waves, 1998*, p. 177
47. Kellerer H, Koch R, Wittig S *Combust. Flame* **120** 188 (2000)
48. Melton L A *Appl. Opt.* **23** 2201 (1984)
49. Gurentsov E V *Nanotechnol. Rev.* **7** 583 (2018)
50. Schulz C et al. *Appl. Phys. B* **83** 333 (2006)
51. Eremin A V, Gurentsov E V, Musikhin S A *J. Alloy Compd.* **727** 711 (2017)
52. Sipkens T A et al. *Appl. Phys. B* **128** 72 (2022)
53. Eremin A V et al. *Appl. Phys. B* **104** 285 (2011)
54. Gurentsov E V, Eremin A V, Mikheyeva E Yu *High Temp.* **55** 723 (2017); *Teplofiz. Vys. Temp.* **55** 737 (2017)
55. Drakon A V et al. *Combust. Explosion Shock Waves* **58** 430 (2022); *Fiz. Goreniya Vzryva* **58** (4) 41 (2022)
56. Gurentsov E V, Drakon A V, Eremin A V, Kolotushkin R N, Mikheyeva E Yu *High Temp.* **60** 335 (2022); *Teplofiz. Vys. Temp.* **60** 374 (2022)
57. Frenklach M, Wang H *Symp. Int. Combust.* **23** 1559 (1991)
58. *Intern. Discussion Meeting and Workshop on Laser-Induced Incandescence*: *Quantitative Interpretation, Modelling, Application*; http://liiscience.org
59. Drakon A et al. *Combust. Flame* **232** 111548 (2021)

60. Hanson R K et al., in *NIST Fuel Summit, Sept. 7 – 10, 2008*
61. Mcmillin B K, Lee M P, Hanson R K *AIAA J.* **30** (2) 436 (1992)
62. Mcmillin B K et al., in *Proc. of the Twenty-Third Symp.* (*Intern.*) *on Combustion, 1990* (Pittsburgh, PA: The Combustion Institute, 1990) p. 1909
63. Campbell M F et al. *Shock Waves* **25** 651 (2015)
64. Hanson R K, in *Proc. of the 19th Intern. Symp. on Shock Waves, 1993*, p. 7
65. Davidson D F, Chang A Y, Hanson R K, in *Twenty-Second Symp.* (*Intern.*) *on Combustion* (Pittsburgh, PA: The Combustion Institute, 1988) p. 1877
66. Koshi M, Yoshimura M, Matsui H *Chem. Phys. Lett.* **176** 519 (1991)
67. Ohmori K et al. *Bull. Chem. Soc. Jpn.* **65** 1317 (1992)
68. Eremin A V et al. *Chem. Phys. Rep.* **17** 1275 (1998); *Khim. Fiz.* **17** (7) 16 (1998)
69. Bhaskaran K A, Roth P *Prog. Energy Combust. Sci.* **28** 151 (2002)
70. Bystrov N S et al. *High Temp.* **62** 705 (2024); *Teplof. Vys. Temp.* **62** 796 (2024)
71. Bystrov N S et al. *Fiz.-Khim. Kinetika Gaz. Dinamike* **25** 1128 (2024)
72. Bystrov N S et al. *Combust. Flame* **258** 113096 (2023)
73. Ferris A M et al. *Combust. Flame* **205** 241 (2019)
74. Susa A J, Zheng L, Hanson R K *Proc. Combust. Inst.* **39** 1793 (2023)
75. Figueroa-Labastida M et al. *Combust. Flame* **260** 113256 (2024)